Journal of Thermal Science Vol.33, No.4 (2024) 1379−1393

https://doi.org/10.1007/s11630-024-1985-1 **Article ID: 1003-2169(2024)04-1379-15**

Comparison of Rotating Stall Warning by Different Methods for Variable Speed Configurations in a Contra-Rotating Compressor

XUE Fei, WANG Yan'gang*, LIU Qian, WU Tong, LIU Hanru

School of Power and Energy, Northwestern Polytechnical University, Xi'an 710072, China

Abstract: Stall in compressors can cause performance degradation and even lead to disasters. These unacceptable consequences can be avoided by timely monitoring stall inception and taking effective measures. This paper focused on the rotating stall warning in a low-speed axial contra-rotating compressor. Firstly, the stall disturbance characteristics under different speed configurations were analyzed. The results showed that as the speed ratio (RR) increased, the stall disturbance propagation speed based on the rear rotor speed gradually decreased. Subsequently, the standard deviation (SD) method, the cross-correlation (CC) method, and the discrete wavelet transform (DWT) method were employed to obtain the stall initiation moments of three different speed configurations. It was found that the SD and CC methods did not achieve significant stall warning results in all three speed configurations. Besides, the stall initiation moment obtained by the DWT method at RR=1.125 was one period after the stall had fully developed, which was unacceptable. Therefore, a stall warning method was developed in the present work based on the long short-term memory (LSTM) regression model. By applying the LSTM model, the predicted stall initiation moments of three speed configurations were at the 557th, 518th, and 333rd revolution, which were 44, 2, and 74 revolutions ahead of stall onset moments, respectively. Furthermore, in scenarios where a minor disturbance preceded the stall, the stall warning effect of the LSTM was greatly improved in comparison with the aforementioned three methods. In contrast, when the pressure fluctuation before the stall was relatively small, the differences between the stall initiation moments predicted by these four methods were not significant.

Keywords: contra-rotating compressor; stall disturbance; stall initiation moment; long short-term memory (LSTM); stall warning

1. Introduction

Stall is a common flow instability phenomenon in axial flow compressors and is considered one of the most serious aerodynamic disasters in turbomachinery, alongside surge [1]. The earliest description of the stall was in Stenning's account [2], where Frank Whittle discovered that it occurred in the compressor when the flow rate decreased during the experiment. Since then, scholars from various nations have conducted extensive and continuous research on this topic. In 1955, Emmons [3] proposed a two-dimensional linear stall model based on the small perturbation theory. This model was still considered a classical explanation for the stall phenomenon. With continuous research on the stall mechanism, Moore and Greitzer [4, 5] developed the

Received: Aug 27, 2023
AE: KAN Xiaoxu

Corresponding author: WANG Yan'gang E-mail: wyg704@nwpu.edu.cn

Nomenclature

A	airflow circulation area	R	rotor
n	rotor speed	r	revolution
P	pressure	RMSE	root mean square error
P^*	normalized pressure	RNN	Recurrent Neural Network
U	blade velocity	RR	speed ratio
V	absolute airflow velocity	SD	Standard Deviation
μ	mathematical expectation	**Subscripts**	
ρ	density	1	front
σ	standard deviation	2	rear
ϕ	flow coefficient	atm	atmosphere
Ψ	pressure rise coefficient	ave	average
Abbreviations		c	current
BPF	blade passing frequency	e	outlet
CC	cross-correlation	i	inlet
DWT	Discrete Wavelet Transform	m	mid-span
IGV	inlet guide vane	pred	predicted value
LSTM	Long Short-Term Memory	s	stall disturbance
PA	prediction accuracy	ts	total to static

M-G model. This model can theoretically predict the existence of large-scale rotating disturbances (modal) in compressors before stall. Subsequently, McDougall et al. [6] used spatial Fourier analysis to process the hot-wire signal and detected modal stall inception in a single-stage axial compressor. In addition, Day et al. [7] identified another type of stall inception (spike) in the compressor experimentally. This type of stall inception usually occurs in the local channel at the top of the rotor blade and develops faster than modal waves. Even today, these two types of stall inceptions are still recognized as the typical forms by the academic community. Furthermore, Day et al. [8] discovered a "fixed position" type of stall inception in three multi-stage high-speed axial compressors. This kind of pre-stall disturbance does not rotate in the circumferential direction and is monitored only 3–4 revolutions before the stall, and then rapidly develops into mature stall cells. In 1998, Freeman et al. [9] discovered that stall inception was a specific disturbance that occurred at 90% of the design speed in an eight-stage high-speed axial flow compressor. This disturbance was fixed at a certain circumferential position and occupied 1/3 of the circumferential range when it first appeared. It did not start to rotate until after 3–4 revolutions. In 2014, Li et al. [10] identified "partial surge" stall inception in a transonic axial flow compressor. This type of stall was located at the rotor hub region and was axisymmetric. The frequency of the pre-stall disturbance was constant during stall development and was detected as early as 3000 r before the stall. Yue et al. [11] conducted experiments in a low-speed axial contra-rotating compressor and found a large-scale, low-speed pre-stall disturbance that was distinct from modal and spike stall inception. After several decades of research, scholars have gained a profound understanding of the stall phenomenon in compressors. However, the problem of how to timely warn and avoid the disaster before the stall occurs remains an urgent issue that needs to be addressed [1].

Extensive studies of stall processes in compressors have revealed that the key flow mechanisms for stall initiation are closely linked to unsteady flow in the rotor blade tip region. Moreover, stall inception in compressors typically occurs first in the blade tip region. Epstein et al. [12] first suggested that the utilization of active control techniques could effectively delay the onset of stall. According to the different types of stall inception, Day adopted different active control strategies based on the air injection at the top of the blade [13]. By monitoring the circumferential position of the disturbance in real-time during the test, the stall inception disturbances were successfully suppressed, and the stall margin was improved by 4% by injecting air at the local position. Du et al. [14] successfully increased the stall margin of a three-stage axial flow compressor by 20% via air injection upstream of the first-stage rotor. The rapid detection of stall inception is critical to the successful application of active control technology. During this process, it is critical to analyze the unsteady signal.

In 1991, Inoue found that there was a sharp unsteady fluctuation in the top region of the blade near the stall, and the periodicity presented in the steady state vanished

[15]. Based on this phenomenon, Park et al. [16] used the cross-correlation (CC) method to analyze the pressure signal and detected a disturbance wave several hundred revolutions before stalling. Researchers widely favor this class of time-domain analysis methods due to their simplicity of calculation and their applicability for online stall monitoring. Furthermore, some frequency-domain analysis methods such as Fast Fourier Transform (FFT), Power Spectral Density (PSD) method, and Wavelet analysis are also widely used to characterize the stall characteristics in a compressor [17–19]. However, these methods are limited by the fact that they cannot reflect the time information of the stall disturbance. Liu et al. [20] compared and analyzed the stall warning performance of auto-correlation, cross-correlation, Root Mean Square (RMS), and Fast Wavelet Transform (FWT) methods under different operating conditions. The results demonstrated that the CC method was independent of the sensor installation location and had good stall warning performance in both distortion and non-distortion regions. The time-frequency analysis method is a signal processing technique that combines the advantages of the time-domain analysis method and the frequency-domain analysis method. Yue et al. [21] developed an empirical modal decomposition (EMD) combined with the local mean decomposition (LMD) method. This method inherits the strong robustness of EMD and the well-defined instantaneous frequency of LMD, so it provides good results in the analysis of stall data with strong nonlinearity. However, its universality is poor as its performance varies greatly under different forms of stall, and it mostly relies on experience in setting the threshold.

In recent years, deep learning has attracted a lot of attention from scholars in various fields due to its ability in learning and fitting strongly nonlinear data sets. Recurrent Neural Network (RNN) is a type of neural network that can be used for forecasting time series, and it has been applied successfully in various fields such as fault diagnosis [22, 23]. Long Short-Term Memory (LSTM) has further improved RNN's ability to remember time series over long periods. Malhorta et al. [24] trained an LSTM with normal time series data set to predict the values of multiple time steps. They then modeled the prediction error as a multivariate Gaussian distribution to obtain the probability of fault occurrence. Results showed that the LSTM obtained favorable results on four different sets of time series data for anomaly detection. Saniat et al. [25] used an LSTM model to learn from 26 400 seconds of data obtained from a simulated aircraft. The study demonstrated that the network model was able to predict aircraft stall warnings with an accuracy of greater than 95% and a lead time of 10 seconds. Hipple et al. [26] compared two models of LSTM (classification and regression) and trained the network model with the speed data of the compressor. Results revealed that the LSTM regression model had a better stall warning performance and was able to give stall warning 5–20 ms before the stall.

From the above literature, it is evident that deep learning has been widely used in nonlinear signal diagnosis. However, compressor stall experiments are usually labor-intensive, resulting in a lack of experimental data available for research. As a result, the application of deep learning technology in compressor stall warning has been delayed. Thus, the dynamic pressure stall time series collected by the high-frequency dynamic pressure sensor array in a low-speed axial contra-rotating compressor at Northwestern Polytechnic University in Xi'an, China are used to develop the rotating stall warning method with neural network. In this paper, the LSTM regression model is trained using the data sets collected from different speed configurations. Then, the best-performing model is used to obtain the stall warning results for three speed configurations. These results are compared with those obtained by the Standard Deviation (SD) method, CC method, and Discrete Wavelet Transform (DWT) method. Finally, the reason why the LSTM regression model is more effective than other methods is explained.

2. Facilities and Measurement

2.1 Test bench

Fig. 1 shows the low-speed axial flow contra-rotating compressor test bench. The aerodynamic structure is inlet guide vanes (IGVs) - front rotor (R_1) - rear rotor (R_2), and the specific parameters are shown in Table 1.

Following the direction of airflow, the front rotor rotates clockwise, and the rear rotor rotates anticlockwise. The negative sign in Table 1 represents clockwise rotation. For the brief discussion below, the front rotor speed will not include a negative sign. The front and rear rotors are respectively driven by two three-phase asynchronous motors with a rated power of 22 kW. To ensure the contra-rotating compressor operates smoothly from a steady state to stall, the rotor speed is controlled using proportional integral derivative (PID) technology to maintain the fluctuation of the shaft speed is no more than 0.2 r/min. By controlling the axial position of the throttle cone at the end of the bench, the flow area of the compressor outlet is changed, and thus the airflow of the compressor is regulated. During the steady state - stall process, the throttle cone moves in a pattern of progressively shorter distance and lower speed with each movement in order to ensure that the stall phenomenon can be captured in time. Fig. 1 shows that there are 9 electromagnetic bleed valves arranged in the circumferential direction of the transition section. These valves can be controlled to bleed in order to achieve a

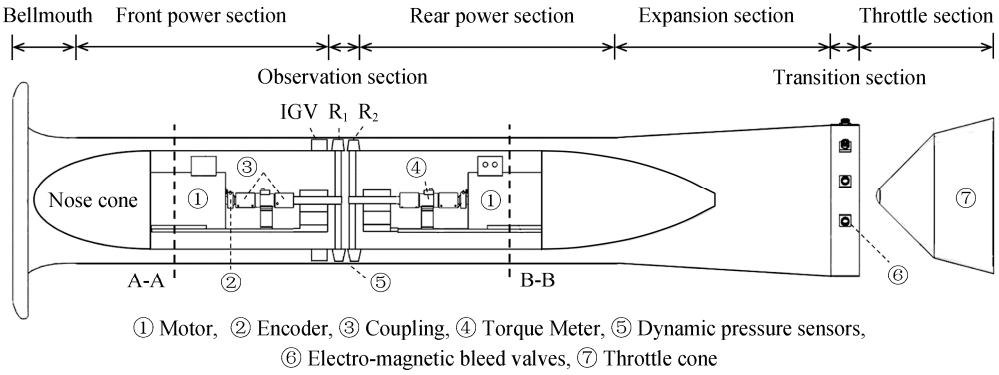

Fig. 1 Overall layout of the contra-rotating compressor test bench

Table 1 The specific parameters of the contra-rotating compressor test bench

Parameters	Value
Number of IGVs	19
Number of R_1 blades	21
Number of R_2 blades	21
R_1 design speed/r·min^{-1}	–2400
R_2 design speed/r·min^{-1}	2400
Hub ratio	0.82
Casing diameter/mm	780
Blade tip clearance/mm	0.5
Flow rate at design point/kg·s^{-1}	6.4
Static pressure rise at design point/kPa	7.0

quick exit from the dangerous working condition when an emergency such as a surge occurs. At the inlet (A-A section) and outlet (B-B section) of the compressor, four static pressure holes are uniformly arranged in the circumferential section to obtain the flow coefficient (ϕ) – total-to-static pressure rise coefficient (Ψ_{ts}) characteristic curve. The calculation process of ϕ and Ψ_{ts} is shown in Eq. (1) and Eq. (3) respectively.

$$\phi = V_i / U_{1m} \tag{1}$$

where V_i is the compressor inlet airflow velocity, and the calculation formula is shown in Eq. (2). U_{1m} is the R_1 medium radial velocity.

$$V_i = \frac{A_i \varepsilon \sqrt{2\rho_{atm}\left(-P_{i,ave}\right)}}{\rho_{atm} A_i} \tag{2}$$

where A_i is the inlet airflow circulation area of compressor; ρ_{atm} is the local atmospheric density, and ε is the expansion coefficient. The numerator in Eq. (2) can be calculated to obtain the inlet airflow mass flow.

$$\Psi_{ts} = \frac{P_{e,ave}}{\frac{1}{2}\rho_{atm} U_{1m}^2} \tag{3}$$

where $P_{e,ave}$ is the average static pressure at the outlet of the compressor, and also the total-to-static pressure rise.

2.2 Characteristic curves and stall disturbance characteristics

Define the speed ratio as RR=$n_1:n_2$, where n_1 represents the front rotor speed, and n_2 represents the rear rotor speed. Taking the design speed (n_1=2400 r/min, n_2=2400 r/min) as an example, Fig. 2 shows the ϕ-Ψ_{ts} characteristic curve. As can be seen from Fig. 2, during the steady-state – stall initiation – fully developed stall – stall recovery – steady-state process, the characteristic curve exhibits a typical hysteresis loop phenomenon, which is depicted by the black dashed box in the enlarged portion. 31 high-frequency response dynamic pressure sensors are arranged in the observation section to collect dynamic pressure data under varying operating conditions. Fig. 3(a) and 3(b) show the arrangement scheme of sensors along both the rotors chord and circumferential direction, respectively. The black cycles in Fig. 3(a) represent two optical fiber sensors used for phase locking. More detailed information about phase-lock system and sensor installation information can be found in Ref. [11]. Using these sensors can obtain the stall disturbance characteristics.

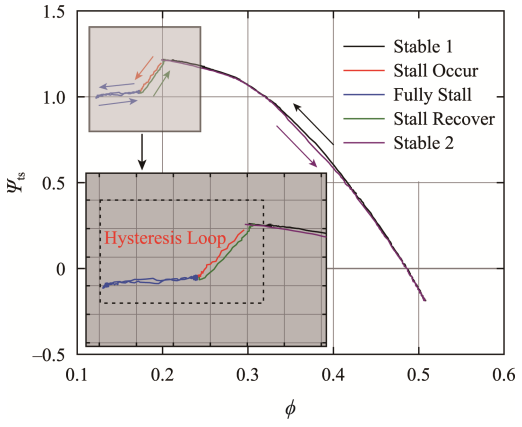

Fig. 2 The ϕ-Ψ_{ts} characteristic curve of contra-rotating compressor (n_1=2400 r/min, n_2=2400 r/min)

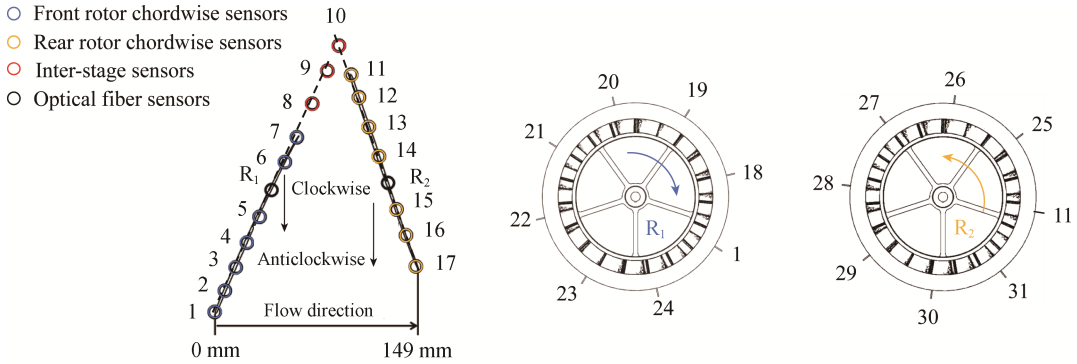

(a) Chordwise layout (b) Circumferential layout

Fig. 3 The layout of the dynamic pressure sensors

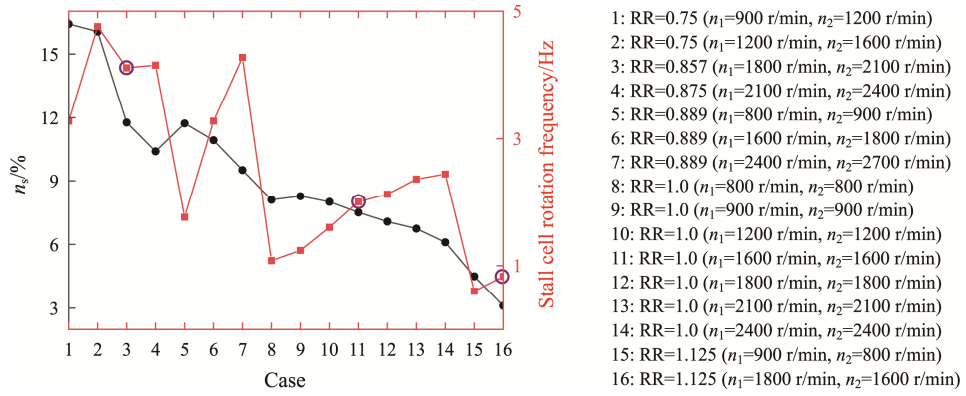

Fig. 4 Stall characteristics of different speed configurations

By analyzing the time-dependent pressure collected simultaneously by sensors, the stall initiation process and its characteristics under different speed configurations can be well understood. When the stall occurs, the position of the throttle cone in the axial direction remains unchanged, while the Ψ_{ts} and ϕ drop sharply at a specific moment. The stall occurrence process and disturbance characteristics of this contra-rotating compressor are detailed in Ref. [11], which provides an example of both front and rear rotor speed of 800 r/min. Previous numerical calculations for this compressor have obtained the evolution of the tip leakage vortex from steady state to stall [27]. This study explains the stall disturbance characteristics and generation mechanism.

The stall characteristics of the contra-rotating compressor can be obtained under different speed configurations by varying the front and rear rotor speeds, as detailed in Fig. 4. The horizontal axis represents different speed configurations, and detailed information is shown on the right side of the figure. It can be found that the stall disturbances under different speed configurations rotate at varying propagation speeds. As the speed ratio increases, the propagation speed of stall disturbances based on rear rotor speed (n_s) decreases gradually. The maximum stall cell rotation frequency does not exceed 5 Hz. Three speed configurations with different stall disturbance characteristics are used to test the generality of stall warning for each method. As shown by purple cycles in the figure, the stall cell rotation frequency of these three speed configurations decreases as the speed ratio increases. The pressure data sets of remaining 13 speed configurations are used as training data for LSTM in subsequent analysis.

3. Stall Warning Results Based on Three Classical Approaches

Prior to the application of the LSTM, several classical stall warning methods are commonly used. To illustrate the effectiveness of LSTM-based stall warning method developed in this paper, we first analyze results obtained by SD method, CC method and DWT method. Different stall warning methods are performed on the pressure data collected by the No. 1 sensor for these three speed configurations. Due to a sensor sampling frequency of 5.12 kHz and a sampling time of 25 s, pressure data length is 128 000.

3.1 Standard deviation (SD) method

The standard deviation of a segment of data reflects the difference between the current data and the overall mean. As the pressure value exhibits significant

fluctuations during a stall event, the SD method can be effectively employed for online monitoring of stalls. The formula is shown in Eq. (4).

$$\sigma = \sqrt{\frac{1}{N}\sum_{i=1}^{n}\left(P_{\mathrm{c}} - P_{\mathrm{ave}}\right)^2} \tag{4}$$

where σ is the standard deviation; N represents the number of samples; P_{c} is the current pressure value and P_{ave} is the average of a segment of pressure data.

Before analyzing the standard deviation of the original data collected by the sensor, these raw data are first filtered using the fifth-order Butterworth low-pass filter to remove high-frequency signals such as blade passing frequency (BPF). The original data collected under different speed configurations are all filtered with 0.33 times front rotor BPF ($\mathrm{BPF_{R1}}$) to eliminate high-frequency signals while maintaining the stall and pre-stall disturbances information [28]. Then the filtered data are normalized to remove the effects of different pressure fluctuation ranges at different speed ratios. Following this, the standard deviation of the pressure time series is calculated for each 25 ms time interval. The resulting standard deviation data has a length of 1000 and is subsequently subjected to a smoothing process. Using an SD threshold of 0.07, stall disturbances can be effectively determined. Fig. 5 reflects the process of stall initiation moments obtained by using the SD method. The black curve is the standard deviation; the red curve is the result after smoothing, and the blue dashed line is the SD threshold and the stall initiation moment. The stall is detected at the 594th, 495th, and 390th revolution for the three speed configurations using the SD method, respectively.

3.2 Cross-correlation (CC) method

Cross-correlation can indicate the degree of signal similarity between a pair of sensors at the same moment [17]. In this study, the pressure collected by the No. 1 sensor and the No. 20 sensor, which are symmetrical in the circumferential direction, are selected for cross-correlation analysis. Take RR=0.857 as an example, Fig. 6 illustrates a comparison of the pressure time domain signals of the two sensors for both steady state (ϕ=0.49) and stall condition (ϕ=0.16). The black and red curves respectively represent the pressure collected by the No. 1 sensor and No. 20 sensor. As shown in the figure, the wall pressure waves of both sensors exhibit a strong periodicity under steady-state condition while displaying a discernible phase difference. In the case of stall condition, the periodicity of the pressure waves is destroyed, and the coincidence is reduced. For this reason, it is feasible to use the CC method as a stall warning method. The calculation is shown in Eq. (5).

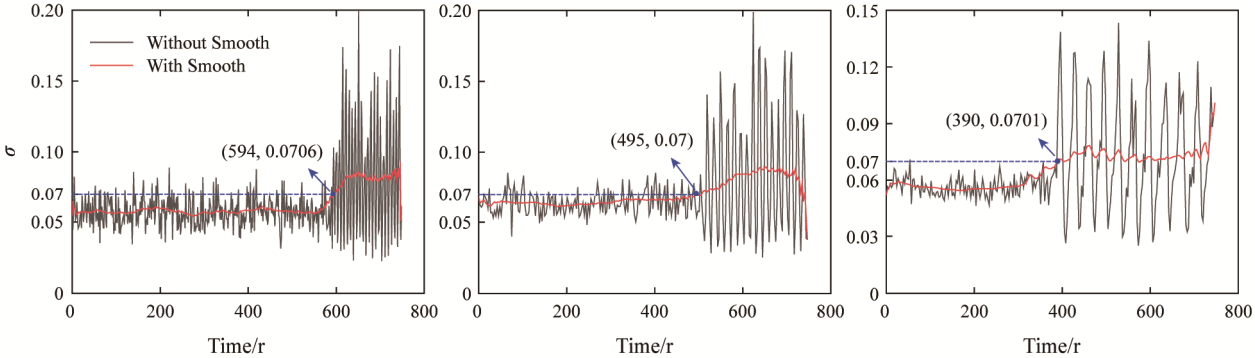

Fig. 5 Stall initiation moments obtained by SD method

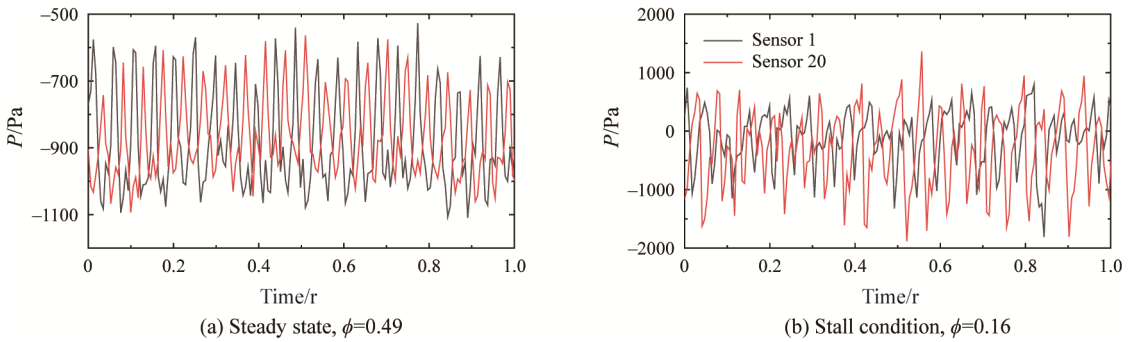

Fig. 6 Comparison of pressure time domain signals collected by two circumferentially symmetric sensors

$$r_{AB}(t)=\frac{\sum_{k=t-\mathrm{wnd}}^{k}A_kB_k}{\sqrt{\sum_{k=t-\mathrm{wnd}}^{k}A_k^2}\sqrt{\sum_{k=t-\mathrm{wnd}}^{k}B_k^2}} \tag{5}$$

where $r_{AB}(t)$ is the cross-correlation value of the pressure signal; A_k and B_k respectively represent the pressure stall time series collected by the two sensors; k represents the discrete time; t is the relative operation time, and wnd represents the length of data in each sliding window.

Before calculating the cross-correlation for different speed configurations, the same fifth-order Butterworth low-pass filter is applied. A smoothing process is then applied to further refine the cross-correlation results. Empirically, a cross-correlation value ($r_{1,20}$, the subscript 1,20 represents the No. 1 and No. 20 sensor) below 0.5 indicates weak correlation between two signals. Thus, a $r_{1,20}$ threshold value of 0.5 is selected to judge the stall initiation moment. Fig. 7 reflects the procedure of obtaining the cross-correlation with stall initiation moments for different speed configurations. The black curve is the cross-correlation; the red curve is the result after smoothing, and the blue dashed line is the stall threshold. Using the CC method for stall warning, it can be found that the compressor stalls at the 572nd, 509th and 395th revolution for three speed configurations of RR=0.857, RR=1.0, and RR=1.125, respectively.

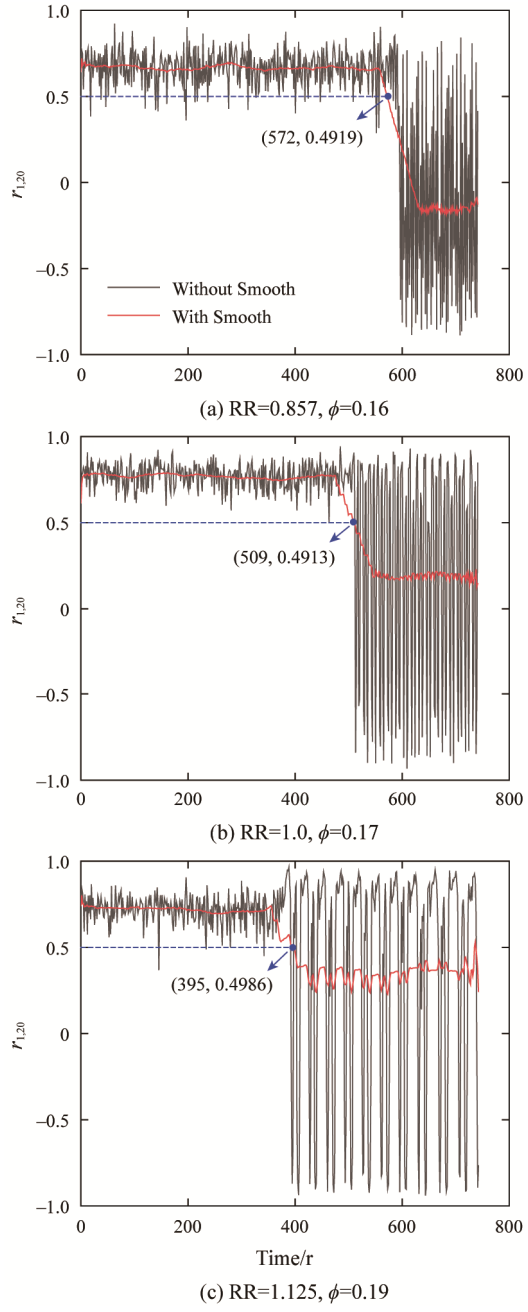

Fig. 7 Stall initiation moments obtained by CC method

3.3 Discrete wavelet transform (DWT) method

DWT is a multi-scale analysis of the signal by decomposing the original signal into high-frequency and low-frequency components [19]. For a practical signal of length N, DWT can only decompose at most $\log_2 N$ layers. The length of pressure collected by the sensor in this paper is 128 000 and therefore can only decompose up to 16 layers. The sampling frequency of the sensor is 5.120 kHz and according to the Nyquist sampling theorem, the highest valid information of the collected pressure does not exceed 2.560 kHz. Fig. 8 illustrates the frequency range of the approximate signal (cA) and the detail signal (cD) for each layer when DWT is performed on the pressure. Fig. 4 indicates that the stall cell rotation frequency gradually decreases as the speed ratio increases. As a result, the number of cD layers containing the stall disturbance information at different speed ratios varies but is less than 16 for all speed configurations, indicating that the DWT method is suitable for stall warning.

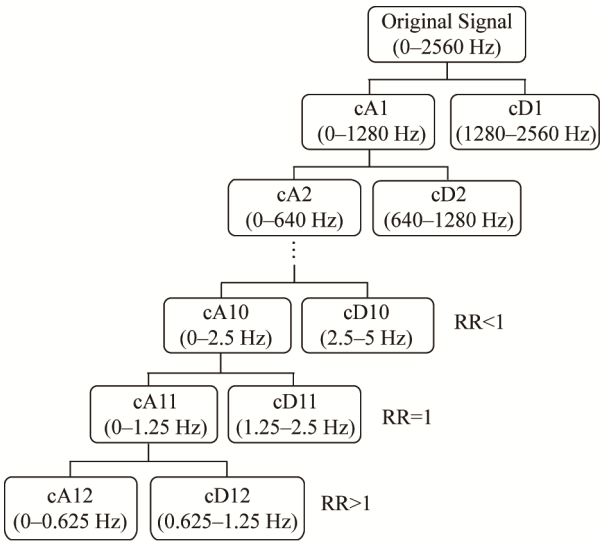

Fig. 8 The DWT decomposition process of the pressure data

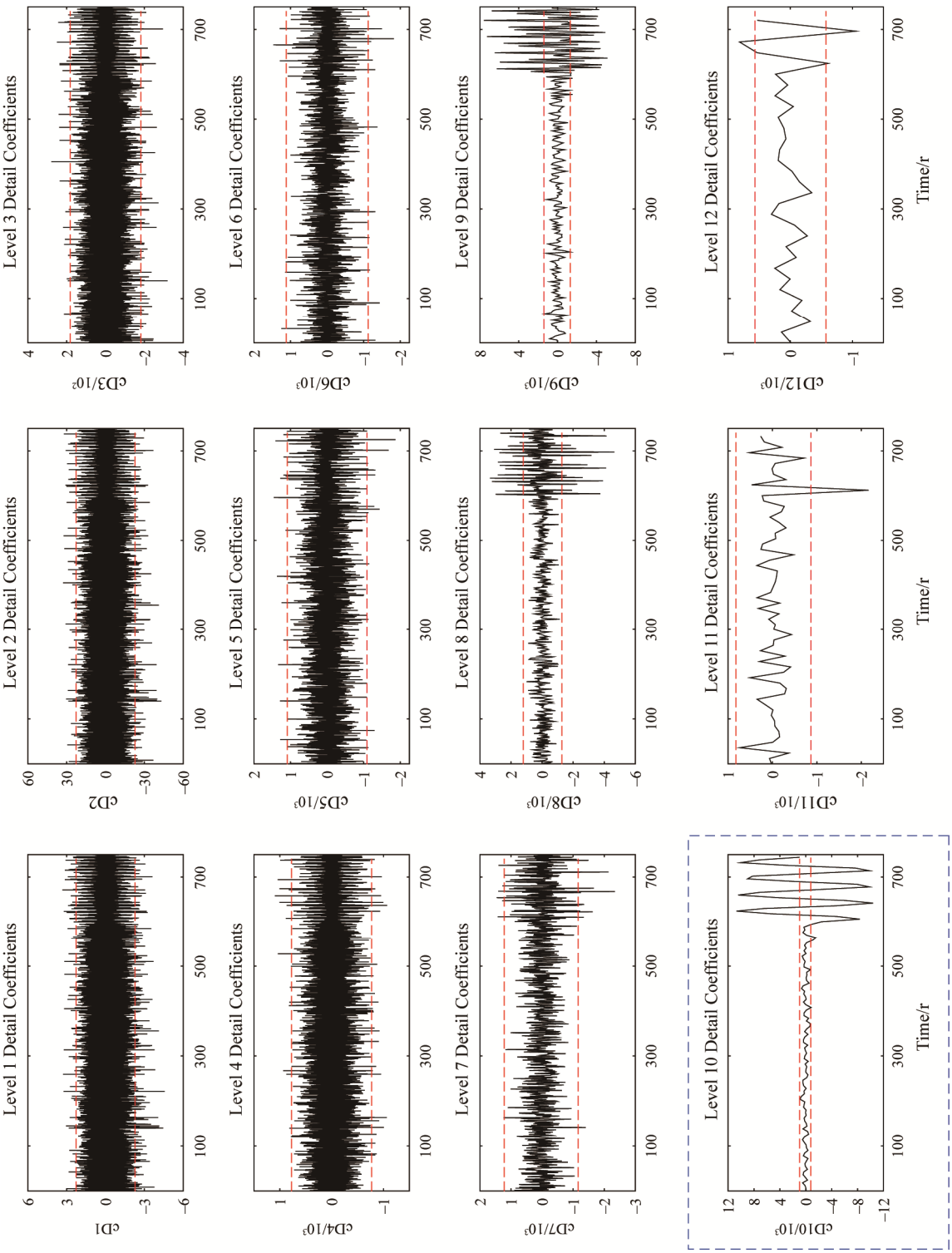

Fig. 9 Each layer of detail signal obtained by DWT at RR=0.857

The original data collected by the sensor are first filtered using the same low-pass filter. Taking RR=0.857 as an example, Fig. 9 shows the cD obtained by DWT processing of the filtered data. The blue dashed box represents the detail signal containing the stall disturbance information, and the red dotted line is the reference line for each layer of the detail signal. Assuming that pressure data obey a normal distribution $N(\mu, \sigma^2)$ in steady state condition, approximately 68.3%, 95.4% and 99.7% of the data will fall within $\mu\pm\sigma$, $\mu\pm2\sigma$, and $\mu\pm3\sigma$, respectively.

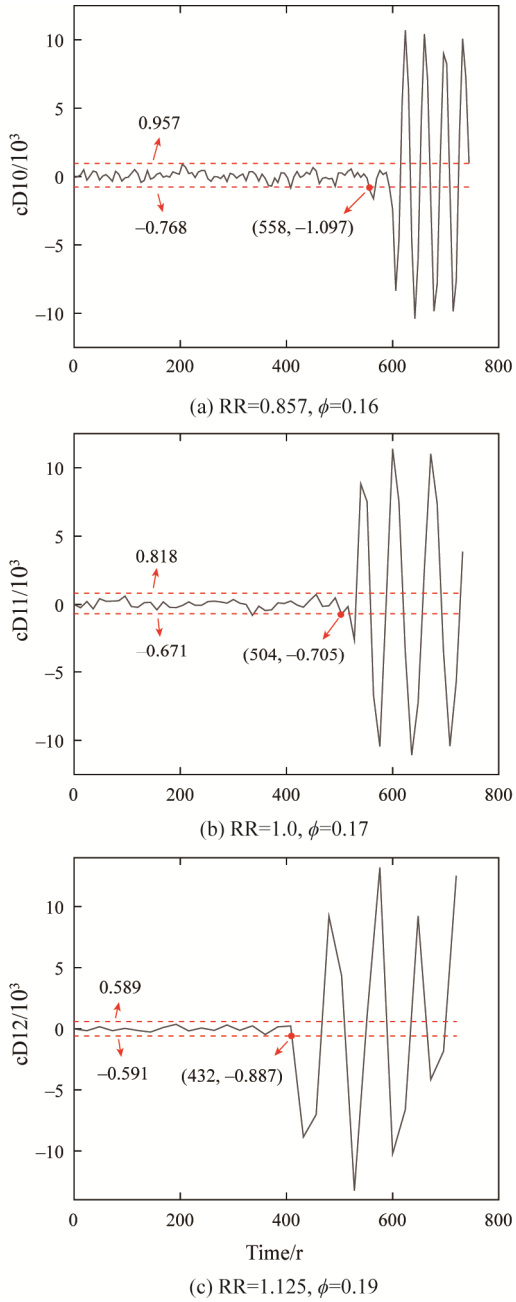

Fig. 10 Stall initiation moments obtained by DWT method

The mathematical expectation μ and the standard deviation σ are calculated using the steady-state data of the first twenty revolutions. Therefore, this paper selects $\mu+3\sigma$ and $\mu-3\sigma$ as the reference lines. Fig. 10 reflects the process of obtaining the stall initiation moments using the DWT method. It can be seen that the compressor stalls at the 558th, 504th, and 432nd revolution for these three speed configurations, respectively.

4. Stall Warning Results based on LSTM Model

4.1 Introduction of the LSTM

The general RNNs are constrained by the Long-Term Dependencies Problem (LTDP), which can result in gradient explosion or gradient disappearance during the error back-propagation process. In order to solve LTDP, the LSTM is developed by adding a new internal state c_t to record historical information up to the current moment. Additionally, three gates are introduced to LSTM to enhance its memory ability, and the calculation formulas are shown in Eq. (6)–Eq. (8). The more detailed operation mechanism of this neural network is shown in Ref. [26], and Fig. 11 shows the structure of the LSTM.

$$f_t = \sigma\left[W_{\mathrm{f}} \cdot \left(h_{t-1}, x_t\right) + b_{\mathrm{f}}\right] \tag{6}$$

$$i_t = \sigma\left[W_i \cdot \left(h_{t-1}, x_t\right) + b_i\right] \tag{7}$$

$$o_t = \sigma\left[W_{\mathrm{o}} \cdot \left(h_{t-1}, x_t\right) + b_{\mathrm{o}}\right] \tag{8}$$

In the above equations, $\sigma(\cdot)$ is the logistic function with the output range of (0, 1); f_t, i_t, o_t are forget gate, input gate and output gate, respectively. W and b are weight matrices and bias terms of these three gates. During the training of the LSTM, the W and b are continuously adjusted through the process of error back-propagation to simulate nonlinear systems. h_{t-1} is the external state of the hidden layer of the previous time step, and x_t is the input parameter of the current time step.

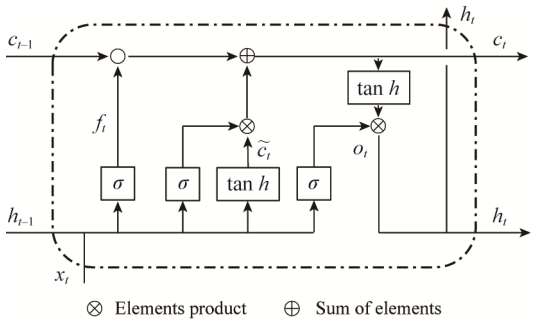

Fig. 11 The cell structure of the LSTM

The c_t can capture critical information and has ability to save this information for a certain time interval. Thus, the LSTM can deal with long-distance dependent time

sequences with higher efficiency than RNNs. The aim of this paper is to provide early warning of the stall before it occurs. The temporal information plays a crucial role in stall warning process. Based on these considerations, the LSTM regression model is selected to investigate contra-rotating compressor stall warning for different speed configurations.

4.2 Dynamic pressure data pre-processing process

Due to noise and other environmental impacts, the pressure collected by the sensors fluctuates significantly, which can lead to divergence in network models if used directly for training. Therefore, the original data need to be pre-processed before they are used to train the neural network models. The procedure is depicted in Fig. 12. To avoid overfitting of LSTM due to sample repetition, only the pressure collected by No. 1 sensor at the leading edge of the front rotor and No. 11 sensor at the leading edge of the rear rotor are employed for LSTM training. The following section illustrates the pre-processing process of the data gathered by No. 1 sensor when the front and rear rotor speeds are 1800 r/min and 2100 r/min, respectively.

Initially, the original data are low-pass filtered with 0.33 times BPF_{R1} by the previously mentioned fifth-order Butterworth low-pass filter. This step helps avoid signal distortion caused by overlapping during later resampling and enhances signal-to-noise ratio. Since the length of pressure data acquired by each sensor is 128 000, and large dimensionality of data for LSTM leading to reduced learning efficiency, a down-sampling method is selected to reduce pressure dimensionality. As a result, the length of the filtered pressure is reduced from 128 000 to 1000, and the sampling frequency is reduced from 5120 Hz to 40 Hz. According to Fig. 4, the maximum stall cell rotation frequency is 4.28 Hz, so the resampled data still satisfy Nyquist sampling theorem. Before the resampled data are learned by network model, the deviation normalization method is applied to eliminate the impact of numerical values on the neural network and enable network to focus more on the autoregressive characteristics and overall trend of data itself.

Fig. 13 reflects the effect of the original pressure data being pre-processed. The black and red curve represents original and resampled pressure, respectively. Define the pressure relative fluctuation amplitude ratio (PRFAR) as the ratio of the pressure fluctuation amplitude during the stall occurrence to the fluctuation amplitude before the stall occurrence. Combined with Eq. (9), the PRFAR of the resampled pressure can be obtained as 4.09, which is four times higher than the 1.01 of the original pressure data. This indicates that the stall disturbance characteristic is highlighted after the raw pressure has been preprocessed, which can improve the learning efficiency and stall prediction performance of the network.

$$\mathrm{PRFAR} = \frac{P_{\mathrm{so,max}} - P_{\mathrm{so,min}}}{P_{\mathrm{bs,max}} - P_{\mathrm{bs,min}}} \tag{9}$$

where the subscript so and bs represent the stall occurrence and before stall occurrence, respectively. So $P_{\mathrm{so,max}}$ represents the maximum pressure value during the stall occurrence, the meaning of the other symbols is in a similar way and will not be explained.

4.3 Training data division and LSTM building

Before training the LSTM regression model, each set of pre-processed data must be constructed as training samples for the network model learning and training. As shown in Fig. 14, the time window length for each

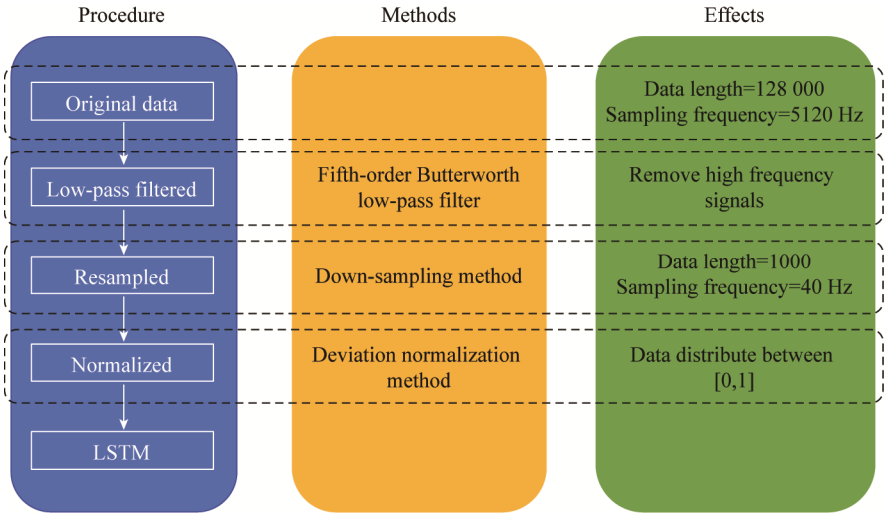

Fig. 12 Original pressure pre-processing process

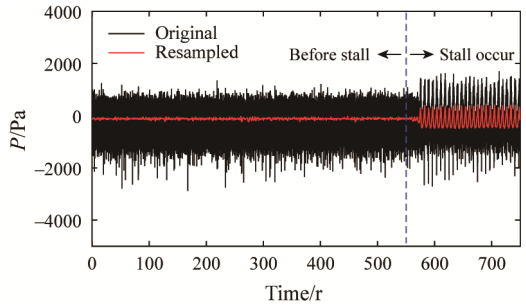

Fig. 13 The original and resampled pressure time series (n_1=1800 r/min, n_2=2100 r/min, ϕ=0.16)

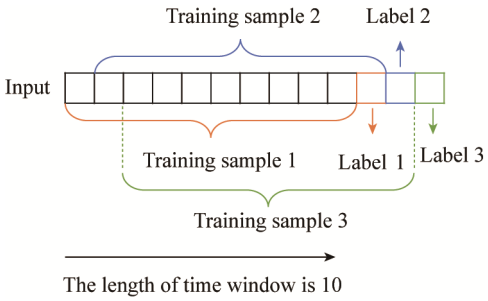

Fig. 14 Diagram of training sample construction

training sample is set to 10 to predict pressure value at the next time step. The figure demonstrates this with training samples and their corresponding labels (same color), with a time interval of 1 between adjacent training samples. After this processing, the size of each training sample is 10 and corresponding label size is 1. Therefore, the length of 1000 resampled data is divided into 990 sets of training samples.

In addition to RR=0.857 (n_1=1800 r/min, n_2=2100 r/min), RR=1.0 (n_1=1800 r/min, n_2=1800 r/min) and RR=1.125 (n_1=1800 r/min, n_2=1600 r/min), which are used to test stall warning performance, the pressure collected at the other speed configurations in Fig. 4 are divided and integrated into training samples. Thus, a total of 25 740 sets of training samples are available. These samples are empirically classified into training and validation sets in a ratio of 7:3. The root means square error (RMSE) of the validation sets is used to evaluate network model performance and give guidance for the adjustment of the hyperparameters. Eq. (10) is the calculation formula.

$$\mathrm{RMSE}=\sqrt{\frac{\sum_{i=1}^{n}\left(P^{*}-P_{\mathrm{pred}}\right)^{2}}{n}} \tag{10}$$

where P^* is the normalized pressure; P_{pred} is the predicted pressure value of the LSTM, and n is the length of the predicted data.

Fig. 15 shows the validation RMSE of the LSTM when adjusting its structure and hyperparameters. It can be inferred that the No. 6 LSTM (LSTM_net6) exhibits the best performance, as evidenced by the smallest validation RMSE of 0.0493. To further demonstrate the advantage of LSTM_net6 in fitting nonlinear pressure, prediction accuracy (PA) is calculated using Eq. (11).

$$\mathrm{PA}=\left(1-\frac{\left|P^{*}-P_{\mathrm{pred}}\right|}{P^{*}}\right)\times 100\% \tag{11}$$

By applying each LSTM model to the same test set, the corresponding predicted pressure values and PA can be obtained. As shown by the red line in Fig. 15, the LSTM_net6 has the highest PA of 89.3%. Therefore, the LSTM_net6 is utilized for stall warning in subsequent analysis. The architecture of LSTM_net6 is as follows: it comprises two layers, with the first layer containing 256 neurons and the second layer containing 32 neurons. The number of Epochs is 200, learning rate is 0.01, and batch size is 256. Since the total number of training sets is 18 018, there will be less than 256 training samples in each epoch which are not learned. To guarantee that LSTM can effectively capture all the data features present in the training sets, we set "Shuffle" as "Every Epoch". Additionally, the LSTM_net6 is optimized using the Adam optimizer, which offers fast convergence and ease of parameter tuning.

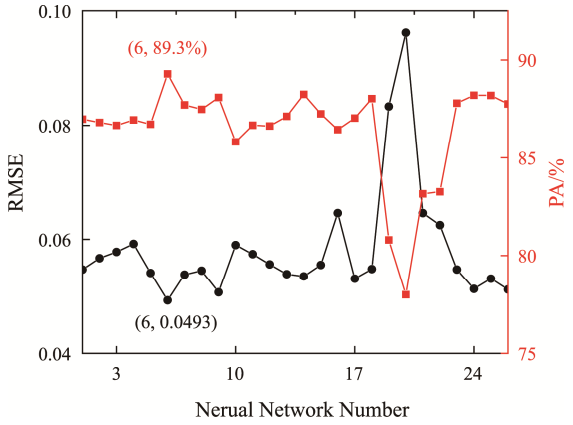

Fig. 15 The performance of LSTM with different hyperparameters

4.4 Stall warning results of LSTM

When rotating stall occurs, a low-pressure stall disturbance rotates in the circumferential direction. This physical phenomenon causes violent pulsation fluctuations in the pressure signal, as can be seen in Fig. 13. The differential method is proven to accurately identify pulsation signals [26]. Fig. 16 shows the recognition results of the differential method for the stall signals in this paper. The black curve is the differential value obtained based on the pressure data predicted by LSTM_net6; the red curve is the resampled data; the red

dashed line is the stall threshold set according to differential value, and the blue dashed lines are the stall occurrence moments. For simplicity of representation, only a small part of the stall occurrence moments is marked in Fig. 16. It can be found that the stall occurrence moments obtained based on the LSTM are consistent with the moments when pressure becomes violently pulsating, indicating that the LSTM can accurately capture the stall in time. Thus, using LSTM_net6 for stall warning is plausible.

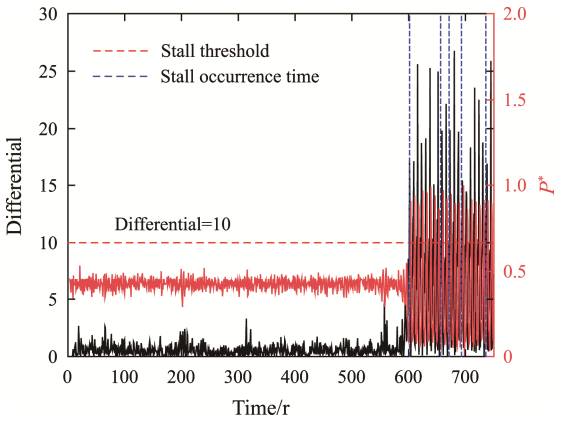

Fig. 16 Stall occurrence moments predicted by LSTM based on differential method (n_1=1800 r/min, n_2=2100 r/min, ϕ=0.16)

The pressure fluctuation range of different speed configurations varies when stall occurs, resulting in a changing distribution range of the differential value. In order to use the same stall threshold to determine the stall initiation moment at different speed ratios and provide an early warning before stall occurs, this paper uses the differential ratio method to obtain the stall threshold. The specific procedure is as follows: the maximum differential value of the first 20 revolutions (steady state) in the pressure time series is taken as the reference. As time passes, the differential ratio is obtained by dividing current differential value with the maximum differential value over elapsed time.

Taking RR=0.857 (n_1=1800 r/min, n_2=2100 r/min) as an example, the subplot at the top of Fig. 17 shows the differential ratio obtained using the original resampled data. The red dashed line is the stall threshold set based on the differential ratio, and the blue dashed line represents the moment when the differential ratio value exceeds the stall threshold for the first time. At a stall threshold of 1.4, the stall initiation moment at this particular speed ratio is found to be the 595th revolution, which corresponds with the moment when the original pressure signals start to exhibit a violent pulsation change, as shown in the subplot at the bottom of Fig. 17. Therefore, this stall threshold of 1.4 is effective in identifying the occurrence of stalls. Henceforth, the differential ratio value of 1.4 can be used as a criterion for determining initiation moment of stall disturbances.

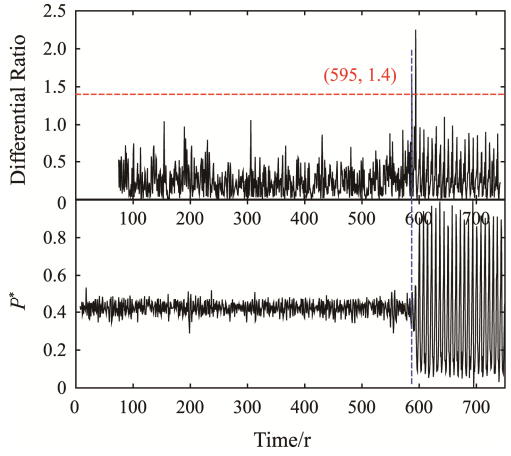

Fig. 17 Stall threshold set based on the differential ratio (n_1=1800 r/min, n_2=2100 r/min, ϕ=0.16)

The LSTM_net6 is used to predict pressure series for different speed configurations. By combining with the stall threshold value set based on the differential ratio, the pressure and corresponding stall initiation moments respectively obtained by the sensor and predicted by LSTM are compared and analyzed, as Fig. 18 shows. The black and red solid lines represent the resampled data and the pressure predicted by the LSTM, respectively. The black and red dashed lines respectively represent the stall initiation moments of the two sets of data.

It can be seen from Fig. 18 that the stall initiation moments predicted by LSTM at RR=0.857 and RR=1.125 are at the 557th and 333rd revolution, respectively. This indicates a significant improvement in stall warning achieved by LSTM, with 44 and 74 revolutions earlier compared to the stall initiation moments obtained based on resampled data. However, LSTM only gains a result of 2 revolutions ahead at RR=1.0. Upon comparing dynamic pressure stall time series data for these three speed configurations, small disturbances before the stall occurs at RR=0.857 and RR=1.125 can be noted. These small disturbances are not prominent in resampled data but are more evident in the pressure predicted by LSTM, as shown in the red rectangular box. At RR=1.0, pressure before the stall is relatively smoother. Based on observed phenomenon, it can be inferred that the LSTM is more sensitive to the small perturbations hidden in the pressure stall time series. This enables it to capture small disturbances before the stall occurs and thus achieve satisfactory stall warning results.

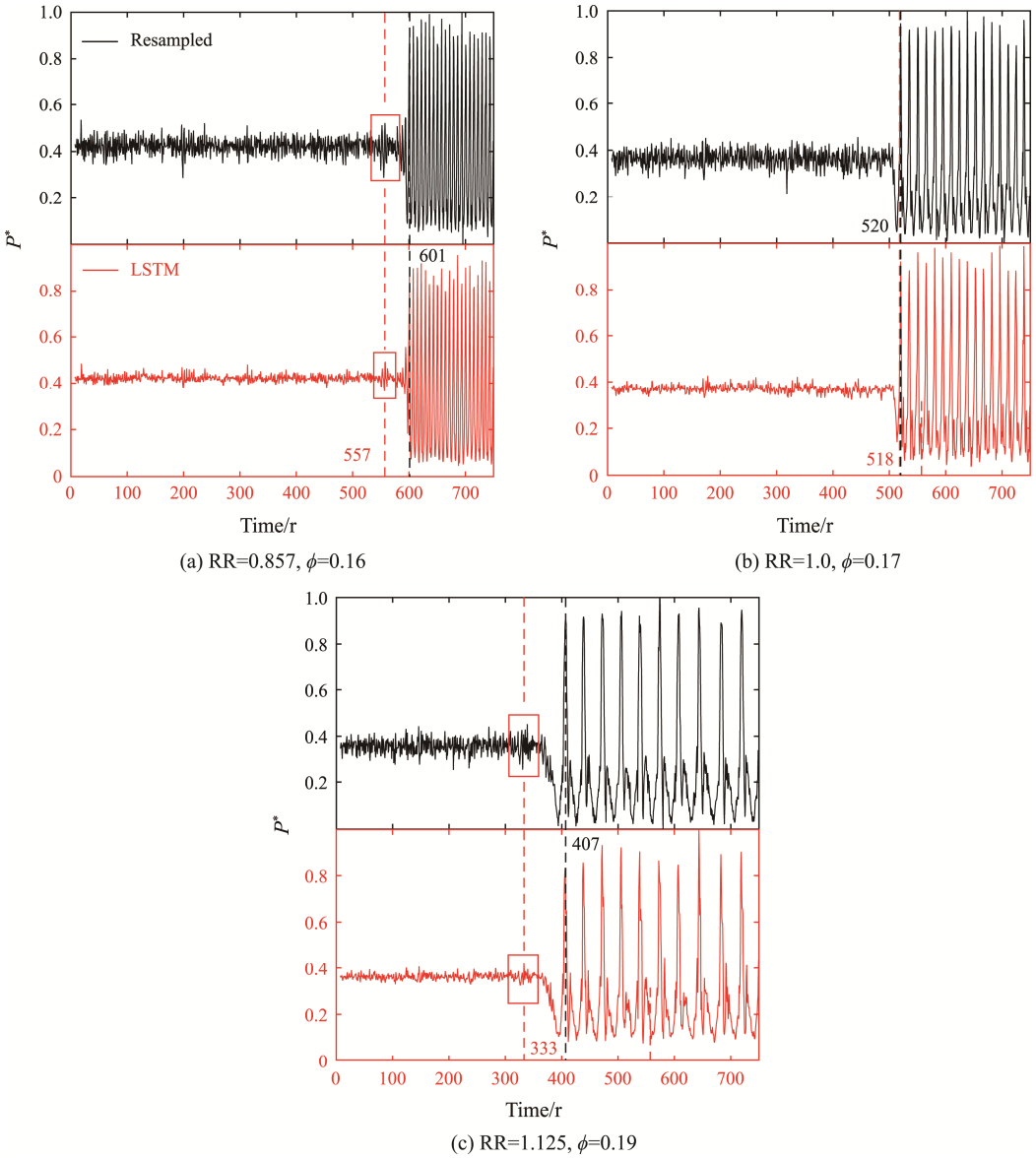

(a) RR=0.857, ϕ=0.16

(b) RR=1.0, ϕ=0.17

(c) RR=1.125, ϕ=0.19

Fig. 18 Stall initiation moments obtained by LSTM

5. Comparison of Stall Warning Results between LSTM and Classical Approaches

In order to analyze more clearly the stall warning performance of the aforementioned methods for different speed configurations, Fig. 19 displays the stall initiation moments of various methods in the pressure stall time series. The red dashed line, blue dashed line, pink dashed line, green dashed line and black dashed line in the figure represent the stall initiation moments obtained by the LSTM model, DWT method, CC method, SD method and original data, respectively.

It can be seen from Fig. 19 that the LSTM has a significant advantage over the other classical methods in terms of stall warning under two speed configurations of RR=0.857 and RR=1.125, and the corresponding stall initiation moments are significantly earlier. This is because the LSTM regression model applied in this paper has the autoregressive properties, which can take into account the change of pressure values over time and react to the small perturbations. Combining the pressure time series data in Fig. 19, it can be found that the pressure has a small fluctuation at a certain moment before the stall in both speed configurations. Moreover, the moment when the LSTM issues the stall warning coincides with the moment where the small fluctuation is located. The SD method and CC method only consider the statistical characteristics within the detection window. The change characteristics of the pressure at the different windows are not correlated. Therefore, only when there is a large fluctuation within the detection window, the global characteristics will change significantly. Then the

corresponding standard deviation and the cross-correlation coefficient exceed the corresponding thresholds, and stall warning will be issued. Therefore, the effectiveness of these two methods is poor compared to the LSTM. Although the DWT method has better stall warning performance than LSTM at RR=0.875 (n_1=2100 r/min, n_2=2400 r/min), it can be found that at RR=1.125, the stall initiation moment obtained by the DWT method is one period after the stall disturbance has fully developed, which is unacceptable. At RR=1.0 (n_1=1800 r/min, n_2=1800 r/min), the advantage of the LSTM for nonlinear time series signal prediction is weakened because the pressure time series data before stall is more stable. As a result, the stall warning performance of various methods is similar.

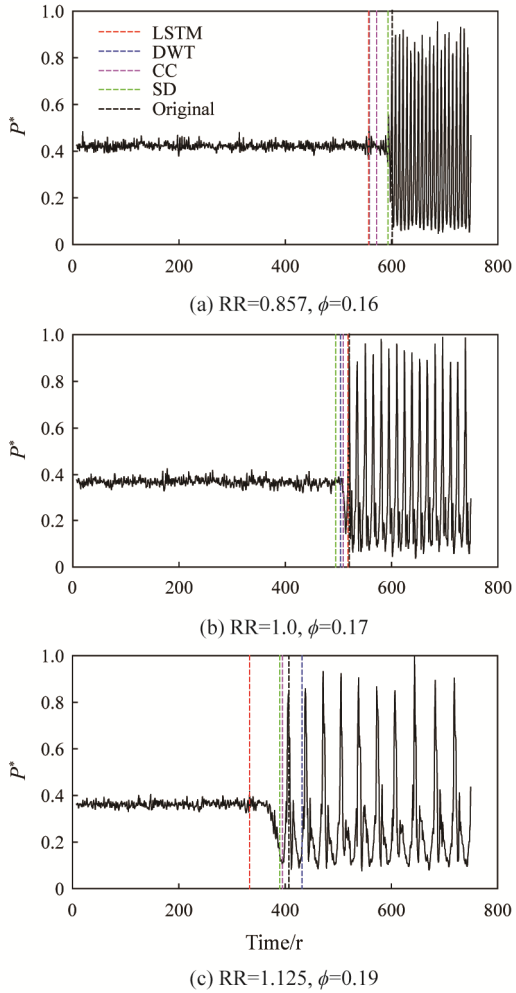

(a) RR=0.857, ϕ=0.16

(b) RR=1.0, ϕ=0.17

(c) RR=1.125, ϕ=0.19

Fig. 19 Comparison of stall warning results of different methods

6. Conclusions

This paper took a low-speed axial contra-rotating compressor as the test object. The characteristic curves and stall initiation characteristics for different speed configurations were obtained and analyzed. Subsequently, the LSTM regression model was trained using pressure stall time series under different speed configurations. The stall warning results of LSTM were then compared with those obtained by the SD method, CC method, and DWT method. Furthermore, an elucidation was provided to explain why the LSTM proved more effective than other stall warning methods. The specific conclusions are as follows:

(1) As the speed ratio increased, the propagation speed of stall disturbances based on the rear rotor speed gradually decreased and the stall cell rotation frequency gradually reduced.

(2) The stall initiation moments predicted by the LSTM at RR=0.857 and RR=1.125 were at the 557th and 333rd revolution, respectively. These instances preceded the stall initiation moments obtained from resampled data by 44 and 74 revolutions. However, the LSTM only gained a stall warning of 2 revolutions ahead at RR=1.0. Based on the pressure time series predicted by LSTM, it could be inferred that the LSTM was more sensitive to the small perturbations hidden in the pressure stall time series.

(3) In predicting stalls for RR=0.857 and RR=1.125, where there were small disturbances prior to the occurrence of stalls, the stall warning performance of LSTM was better than the SD method and CC method. Although the DWT method had a better stall warning performance than the LSTM at RR=0.875, the stall initiation moment obtained by this method was one period after the stall disturbance had fully developed at RR=1.125, which was obviously unacceptable. When both front and rear rotor speed were 1800 r/min, the pressure fluctuation before stall was relatively small. This made the advantage of the LSTM not exploited, and the stall warning performance of various methods did not differ greatly.

Acknowledgements

This work has been supported by the National Natural Science Foundation of China (Grant No. 52276039).

Conflict of Interest

On behalf of all authors, the corresponding author states that there is no conflict of interest.

References

[1] Day I.J., Stall, surge, and 75 years of research. Journal of Turbomachinery, 2016, 138(1): 011001.

[2] Stenning A.H., Stall propagation in cascades of air-foils. Journal of the Aeronautical Sciences, 1954, 21(10): 711–713.
[3] Emmons H.W., Pearson C.E., Grant H.P., Compressor surge and stall propagation. Journal of Turbomachinery, 1955, 77(4): 455–469.
[4] Moore F.K., Greitzer E.M., A theory of post-stall transients in axial compressors-part I: development of the equations. Journal of Engineering for Gas Turbines & Power, 1986, 108(1): 68–76.
[5] Greitzer E.M., Moore F.K., A theory of post-stall transients in axial compression systems: part II—application. Journal of Engineering for Gas Turbines & Power, 1986, 108(2): 231–239.
[6] McDougall N.M., Cumpsty N.A., Hynes T.P., Stall inception in axial compressors. Journal of Turbomachinery, 1990, 112(1): 116–123.
[7] Day I.J., Stall inception in axial flow compressors. Journal of Turbomachinery, 1993, 115(1): 1–9.
[8] Day I.J., Breuer T., Escuret J., et al., Stall inception and the prospects for active control in four high-speed compressors. Journal of Turbomachinery, 1999, 121(1): 18–27.
[9] Freeman C., Wilson A.G., Day I.J., et al., Experiments in active control of stall on an aeroengine gas turbine. Journal of Turbomachinery, 1998, 120(4): 637–647.
[10] Li Q.S., Pan T.Y., Li Z.P., et al., Experimental study of compressor instability inception in a transonic axial flow compressor. Proceedings of the ASME Turbo Expo 2014: Turbine Technical Conference and Exposition, 2014, Paper No: GT2014-25190.
[11] Yue S.Y., Wang Y.G., Wei L.G., et al., Experimental investigation on the development process of large-scale low-speed stall disturbance in contra-rotating compressor. Journal of Thermal Science, 2020, 29(5): 1282–1291.
[12] Epstein A.H., Ffowcs J.E., Greitzer E.M., Active suppression of aerodynamic instabilities in turbomachines. Journal of Propulsion and Power, 1989, 5(2): 204–211.
[13] Day I.J., Active suppression of rotating stall and surge in axial compressors. Journal of Turbomachinery, 1993, 115(115): 40–47.
[14] Li J.C., Liu Y., Du J., et al., Implementation of stability-enhancement with tip air injection in a multi-stage axial flow compressor. Aerospace Science and Technology, 2021, 113(1): 106646.
[15] Inoue M., Kuroumaru M., Iwamoto T., et al., Detection of a rotating stall precursor in isolated axial flow compressor rotors. Journal of Turbomachinery, 1991, 113(2): 281–287.
[16] Park H.G., Unsteady disturbance structures in axial flow compressor stall inception. Dissertation for the Master's degree. Massachusetts Institute of Technology, 1994.
[17] Yue S.Y., Wang Y.G., Wei L.G., et al., Experimental investigation of the unsteady tip clearance flow in a low-speed axial contra-rotating compressor. Proceedings of the ASME Turbo Expo 2018: Turbomachinery Technical Conference and Exposition, 2018, Paper No: GT2018-76055.
[18] Yue S.Y., Wang Y.G., Zhang Z., et al., Experimental investigation of rotating instability in a contra-rotating axial flow compressor. The Aeronautical Journal, 2021, 125(1286): 742–762.
[19] Liu Y., Li J.C., Du J., et al., Application of fast wavelet analysis on early stall warning in axial compressors. Journal of Thermal Science, 2019, 28(5): 837–849.
[20] Liu Y., Li J.C., Du J., et al., Reliability analysis for stall warning methods in an axial flow compressor. Aerospace Science and Technology, 2021, 115(1): 106816.
[21] Yue S.Y., Wang Y.G., Wei L.G., et al., The joint empirical mode decomposition-local mean decomposition method and its application to time series of compressor stall process. Aerospace Science and Technology, 2020, 105: 105969.
[22] Thomas K., Gottfried R., Time series forecasting using neural networks. Proceedings of the international conference on APL. Association for Computing Machinery, New York, USA, 1994, 25(1): 86–94.
[23] Talebi N., Sadrnia M.A., Darabi A., Robust fault detection of wind energy conversion systems based on dynamic neural networks. Computational Intelligence and Neuroscience, 2014, 2014(1): 580972.
[24] Malhotra P., Vig L., Shroff G., et al., Long short term memory networks for anomaly detection in time series. 23rd European Symposium on Artificial Neural Networks, Computational Intelligence and Machine Learning, 2015.
[25] Saniat T.S., Goni T., Galib S.M., LSTM recurrent neural network assisted aircraft stall warning for enhanced situational awareness. 2020, arXiv preprint arXiv: 2012.04876.
https://doi.org/10.48550/arXiv.2012.04876
[26] Hipple S.M., Bonilla A.H., Pezzini P., et al., Using machine learning tools to predict compressor stall. Journal of Energy Resources Technology, 2020, 142(7): 070915.
[27] Chen W.X., Wang Y.G., Wang H., Investigation of the unsteady disturbance in tip region of a contra-rotating compressor near stall. Journal of Thermal Science, 2019, 28(5): 962–974.
[28] Payyappalli M., Pradeep A.M., Pre-stall waves: precursors to stall inception in a contra-rotating axial fan. Proceedings of the ASME Turbo Expo 2020: Turbomachinery Technical Conference and Exposition, 2020, Paper No: GT2020-14371.